DESIGN AND RESEARCH ON THE TRIGGERING MECHANISM OF ROPE FEEDING IN REED BALING DEVICE
/
芦苇打捆装置触发送绳机构的设计和研究

Yang BAI[1)], Xiang ZHENG[2)], Kun LU[3)], Yanjun LI[1)], Jian SONG[1)], Fuxiang XIE*[1)]
[1)]School of Machinery and Automation, Weifang University, Weifang/China;
[2)]BEIQI FOTON MOTOR CO., LTD
[3)]The Affiliated Qingdao Third People's Hospital of Qingdao University
Tel: 13260170996; E-mail: baiyang19891014@163.com
Correspondent author: Fuxiang XIE

DOI: https://doi.org/10.35633/inmateh-76-80

Keywords: *Rope-Feeding Trigger, Reed, Baling, Orthogonal, Kinematic simulation*

ABSTRACT
To enhance the efficiency and quality of whole-stalk reed harvesting and baling while addressing the issues of low efficiency, reed damage, and high fragmentation rate in manual baling, existing mechanical research primarily focuses on harvesting improvements and straw baling equipment optimization. However, it has not yet resolved the coordination problem of achieving both low damage and high efficiency during whole-stalk reed baling. This paper concentrates on a key aspect of reed baling devices by designing and optimizing a trigger rope-feeding mechanism. This mechanism comprises a triggering mechanism and a rope-feeding mechanism. The triggering mechanism employs a combination of a rocker-slider mechanism and springs to achieve reliable triggering and resetting of the baling action. The rope-feeding mechanism utilizes a crank-rocker mechanism to drive the rope-feeding needle, completing tasks such as rope delivery, knotting initiation, and reed compression to enhance bale compactness. A 3D model of the mechanism was established using SolidWorks, and kinematic simulation and parameter optimization were performed using ADAMS. The key parameter combinations for the trigger mechanism rocker length of 100 mm, connecting rod length of 30 mm, offset distance of 90 mm, and the rope feeding mechanism crank length of 160 mm, rocker length of 175 mm, and connecting rod length of 630 mm were determined. Based on the optimization results, orthogonal experiments were conducted with rope type, operating speed, and pre-tightening force as factors. The results indicate that the optimal parameter combination is nylon rope, operating speed of 90 r/min, and pre-tightening force of 123 N. Experimental analysis revealed that operating speed has the most significant impact on productivity, pre-tightening force is the dominant factor influencing the damage rate, and rope type primarily affects the bale forming rate. Bench tests verified that this trigger rope-feeding mechanism effectively enables low-damage, high-efficiency reed baling, significantly improving bale density and operational efficiency, providing new technical insights for the development of reed baling devices.

摘要
为提升芦苇整杆收获打捆的效率与质量，解决人工打捆效率低、易损伤芦苇且破碎率高的问题，现有机械研究主要集中于收割环节及秸秆打捆设备改进，尚未解决整秆芦苇成捆时的低损伤与高效协同问题，本文聚焦芦苇打捆装置的关键环节，设计并优化了一种触发送绳机构。该机构由触发机构和送绳机构组成，触发机构采用摇杆滑块机构与弹簧的组合，实现打捆动作的可靠触发与复位；送绳机构基于曲柄摇杆机构驱动送绳针，完成捆绳递送、打结触发以及对芦苇的挤压，增强草捆紧实度。利用 SolidWorks 建立机构三维模型，通过 ADAMS 进行运动学仿真与参数优化，确定了触发机构摇杆长度 100 mm，连杆长度 30 mm，偏置距离 90 mm，以及送绳机构曲柄长度 160 mm，摇杆长度 175 mm，连杆长度 630 mm 的关键参数组合。基于优化结果，以捆绳类型、工作转速和预紧力为试验因素，进行正交试验。结果表明，最优参数组合为尼龙绳、工作转速 90 r/min、预紧力 123N。试验分析显示工作转速对生产率影响最显著，预紧力是损伤率的主控因素，捆绳类型则主要影响成捆率。台架试验验证了该触发送绳机构能够有效实现芦苇的低损伤高效打捆，显著提高草捆密度和作业效率，为芦苇打捆装置的研发提供了新的技术思路。

INTRODUCTION

Reed, as a high-quality biological resource, has extensive applications in ecology, landscaping, animal husbandry, and other fields *(Zhao et al., 2021)*. Large-scale reed cultivation presents challenges not only in harvesting but also in post-harvest baling. Harvesting whole, intact reed stalks maximizes the strength, fiber integrity, and appearance of the raw material for uses such as weaving and papermaking, while also facilitating efficient storage, transportation, and processing, thereby optimizing resource utilization and economic benefits *(Wang et al., 2023)*. Current reed baling devices are far from meeting baling demands, with manual baling being predominant. Manual baling is not only inefficient but also prone to causing injuries.

Progress has been made in reed harvesting technology through innovative designs. *Du et al. (2024)* developed a reed clamping and conveying device, conducted modal analysis on its frame structure to identify natural frequencies and comprehensively assess external excitation impacts, ultimately validating the design effectiveness through comparative analysis. *Li et al. (2020)* addressed the practical problem of entanglement between reeds and weeds during harvesting by designing a reed harvesting device that links spatial and planar linkage mechanisms. This device achieves synchronous horizontal and vertical cutting within one rotation of the crank shaft, completing coordinated cutting through trajectory analysis of reciprocating vertical and horizontal blades. Their concept of separating transverse reed cutting from longitudinal weed cutting offers insights for aquatic weed cleaning machinery design. *Li et al. (2021)* further studied the conveying tines and motion mechanism post-cutting in reed harvesters, planning a crank-link mechanism with quick-return characteristics to achieve an arcuate trajectory for the tines and validating frame stability through simulation. Considering the characteristics of reeds in southern China, designed a crawler self-propelled reed harvester with a dedicated clamping and conveying device. They analyzed key components, enabling the transport of cut reeds from the front header to the rear, and determined the optimal working parameter combination for the conveying device *(Yin et al., 2023)*. Based on reed compression characteristic experiments, *Chen et al. (2020)* determined the theoretical optimal compression density and corresponding pressure, conducted parametric design of a compression baling device, verified mechanism strength, and identified potential resonance frequencies.

Research on the bundling, compression, and twine feeding stage of reeds, both domestically and internationally, remains relatively scarce, necessitating reference to the structural optimization of bundling mechanisms in other equipment (*Zhong Chengyi et al., 2023, Flick et al., 2019, Nalobina et al., 2024*). Regarding the load issue of the knotter's key component, the knotter jaw, twine tension data and application points were obtained through straw baling tests combined with comprehensive measurement methods. A load conversion model was constructed, revealing that the upper jaw bears the maximum load reaching... Based on this, finite element analysis was conducted, identifying high stress concentrations at the roller shaft mounting point and the corner of the upper jaw (*Chen et al., 2015*). *Zhang et al. (2022)* addressed vibration issues caused by large inertial forces in the reciprocating compression mechanism of large square balers using model optimization, achieving a bale density of 230 kg/m³. *Wang et al. (2021)* utilized MATLAB for kinematic simulation analysis of the feeding mechanism in a 4YF-1300 large square baler, improving the filling capacity of the pre-compression and compression chambers to enhance efficiency. Based on the working principle of the square baler's compression mechanism, combined with motion simulation analysis of the constructed model using ADAMS, the bale density and operational efficiency of the baler were enhanced conducted static and modal simulation analysis on the feeding mechanism and validated the results through field tests *(Zhang et al., 2024; Wang et al. 2025)*. The results indicated stable operation of the feeding mechanism, with no resonance phenomena, faults, and the formation of straw bales with regular shape and high density after operation.

Unlike fragmented forage baling, whole-stalk reed baling requires consideration of baling success rate and fragmentation. More importantly, effectively achieving low-damage, whole-stalk reed harvesting in practice still poses significant technical challenges. This paper addresses the reed baling problem by developing a trigger rope-feeding mechanism for a reed baling device. The trajectory was validated through simulation, and the mechanism was optimized based on reed physical properties. Parameters were optimized, and the baling process was verified through orthogonal experiments considering three factors: rope type, operating speed, and pre-tightening force. This approach aims to improve reed baling efficiency, reduce labor intensity, minimize reed damage during baling, enhance baling efficiency and quality, and validate the mechanism through bench tests, providing new ideas for reed baling device design.

MATERIALS AND METHODS

Design of the Trigger Rope-Feeding Mechanism for Reed Baling Device

The trigger rope-feeding mechanism is a critical component of the reed baling device, and its rationality directly affects baling success. It mainly consists of a triggering mechanism and a rope-feeding mechanism. The triggering mechanism includes a transmission part and springs, while the rope-feeding mechanism comprises a transmission part and a rope-feeding needle. Its primary function is to ensure intermittent motion of the rope-feeding mechanism. This study focuses on kinematic simulation and parameter optimization of the transmission mechanism within the triggering mechanism.

For the triggering mechanism, considering the structural characteristics of the four-bar linkage, the design requirements of the reed baling device, and the design intent requiring the trigger crank to rotate no more than 40°, a combination of a rocker-slider mechanism and springs was adopted. The 3D model and physical diagram of the triggering mechanism are shown in Fig. 1.

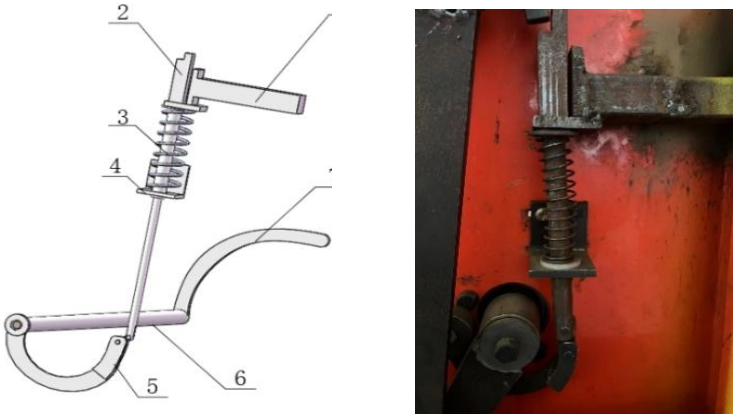

(a) SolidWorks 3D model (b) Physical prototype

Fig. 1 – Trigger mechanism assembly

1. Blocking bracket;2. Blocking rod; 3. Spring; 4. Spring stop block; 5. Connecting plate; 6. Shaft; 7. Trigger crank

The rope-feeding mechanism primarily consists of a crank-rocker mechanism, a rope-feeding needle connecting shaft, and the rope-feeding needle itself. Its 3D assembly is shown in Fig. 2. This mechanism is mainly used to deliver one end of the binding rope into the knotter to complete knotting and simultaneously compress the reed stalks during knotting to enhance bale compactness. The rope-feeding needle is fixed to a rotating shaft. When baling is triggered, the shaft, driven by the crank-rocker mechanism, causes the rope-feeding needle to rotate 90°, delivering the rope into the D-type knotter while simultaneously driving the gear disc *(Cen et al., 2020)*. After knotting is completed, the rope-feeding needle returns to its original position. An additional function of the rope-feeding needle is that its tip blocks reeds fed by the tine, preventing them from being pulled back.

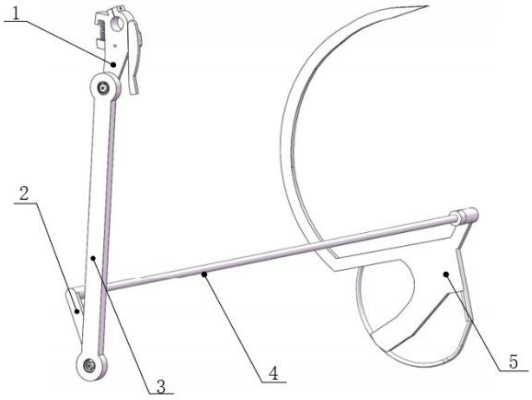

Fig. 2 – Rope-feeding mechanism assembly

1. Crank; 2. Rocker; 3. Connecting rod; 4. Shaft; 5. Rope-feeding needle

The crank of the rope-feeding mechanism is a key component controlling its operation; its shape and size critically affect the successful operation of baling. When the reed reaches the baling weight, the spring on the blocking rod is compressed to its working length, causing the blocking rod in the trigger mechanism to lose its blocking effect on the crank, thus triggering baling. The dimensions of the crank, rocker, and connecting rod were designed based on crank-rocker mechanism calculation formulas, resulting in a crank length of 160 mm, connecting rod length of 630 mm, and rocker length of 175 mm. The rope-feeding needle was designed according to the knotter position. Its main functions are to deliver the rope into the knotter and compress the reeds during baling to make the bale tighter and denser. Therefore, it requires a reasonable curvature and a hollow center for threading the rope *(He et al., 2017)*. Based on the designed 3D model, the working process of the trigger rope-feeding mechanism is shown in Fig. 3.

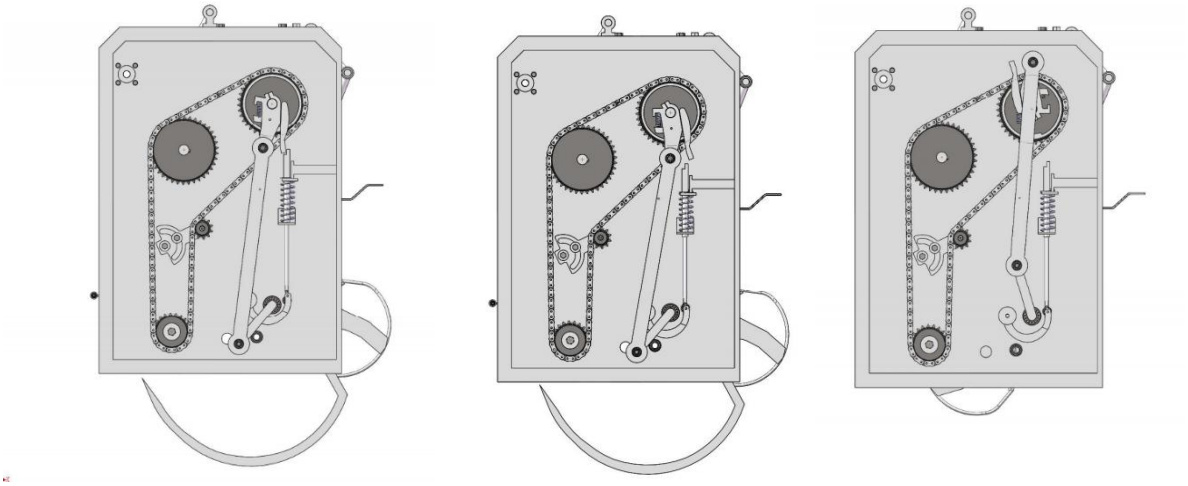

(a) Trigger mechanism blocking crank (b) Trigger mechanism triggering (c) Rope feeding needle feeding rope

Fig. 3 – Triggering the working process of the rope feeding mechanism

Simulation Analysis of Trigger Rope-Feeding Mechanism

The primary function of the triggering mechanism is to pull down the stop block when the trigger crank rotates, initiating the baling action, and then return to the initial position. A combination of an offset rocker-slider mechanism and springs was selected for this purpose. When the force on the trigger crank is transmitted to the rocker, it pulls down the blocking block via the connecting rod, triggering the baling mechanism. Subsequently, the elastic deformation of the spring returns the blocking block to its original position. Since the mechanism includes a spring, it must be mounted vertically with one end fixed during operation to prevent spring offset affecting the experiment. A Cartesian coordinate system for the rocker-slider mechanism was established, as shown in Fig. 4. The geometric relationships of the parameters are according to relation (1).

$$\left(x_B - x_C\right)^2 + \left(y_B - y_C\right)^2 = b^2 \tag{1}$$

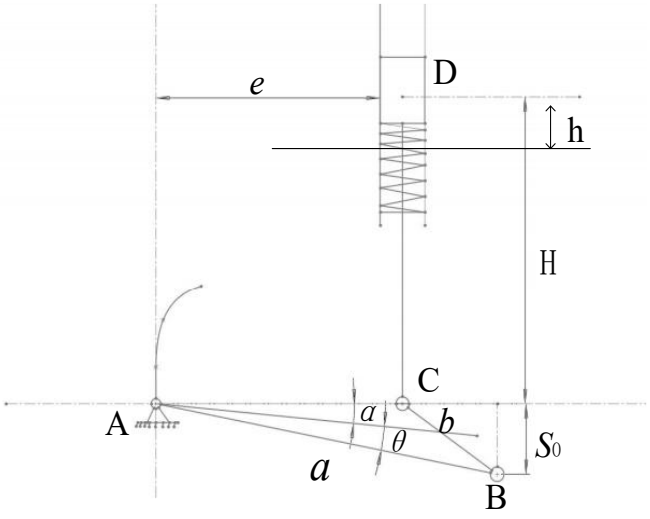

Fig. 4 – Motion diagram of trigger mechanism

In the figure, a is the length between AB, b is the length between *BC*, α is the initial rotation angle of the rocker, θ is the angle of rotation of the rocker. The coordinate of point B is: $(x_B = a\cos\theta; y_B = a\sin\theta)$, point C is (e, S_0), and point D is (e, H) as shown in Table 1.

Substituting the coordinate values into Eq. (1) yields the relationship between the parameters to be determined and the given parameters. To determine the five unknown parameters *a, b, e,* α and S_0, the solving process is simplified by setting $\alpha = 0$, $S_0 = 0$, reducing the unknowns to three. The simplified equation is according to relation (2).

$$2aH\cos\theta - 2ae\sin\theta - \left(a^2 + e^2 - b^2\right) = H^2 \quad (2)$$

Table 1

Design point constraint condition

Design point	X/mm	Y/mm	Z
A	0	0	0
B	$a\cos\theta$	$a\sin\theta$	0
C	*e*	S_0	0
D	*e*	*H*	0

The design variable H = 200 mm. Initial values and variation ranges of each design variable are listed in Table 2. The optimized link lengths must fall within the specified ranges.

Table 2

Initial value of design variable and its constraint conditions

Design point	X/mm	Constraint conditions
a/mm	100	-20.0; 20.0
b/mm	50	-20.0; 20.0
e/mm	100	-20.0; 20.0
θ /°	20.0	0; 40.0

The tension on the blocking block during operation originates from the torque transmitted from the trigger crank to the rocker. The design lengths of *a, b*, and *e* affect the force exerted by the transmission mechanism on the spring. Therefore, ADAMS software was used to simulate the mechanism, with the link lengths of the transmission mechanism as optimization targets, to investigate the influence of design variables on trigger mechanism performance. Using Fig. 4 and Tables 1 & 2, a virtual prototype of the trigger mechanism was built. After adding constraints and setting the rocker as the driving part, simulation was performed. Fig.5(a) shows the initial working position of the transmission mechanism; (b) shows the rocker at the working position, where the blocking block is pulled down 15 mm.

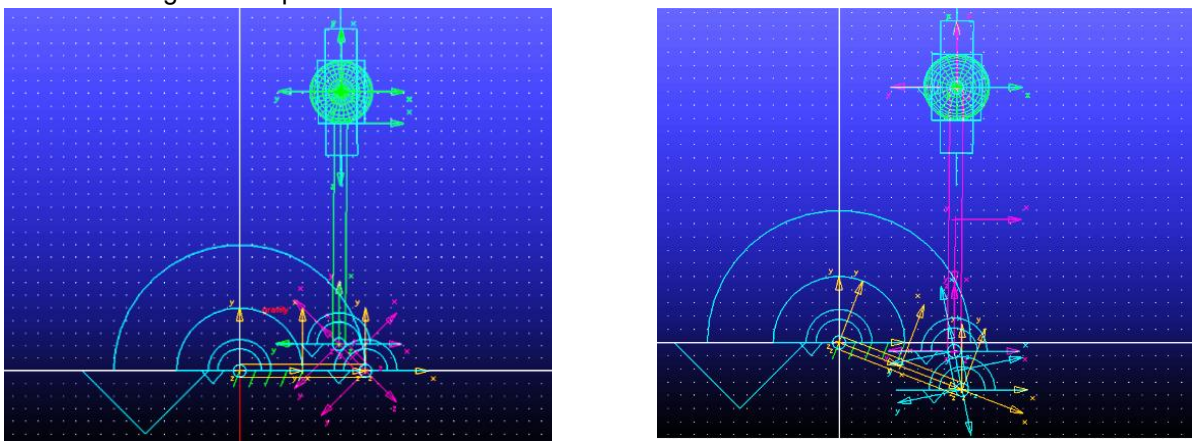

(a) Initial position of joystick (b) Working position of joystick

Fig. 5 – Working position of transmission mechanism

Based on force calculations for the feeding mechanism tines, the torque on the trigger crank during triggering was approximately 14.6 N·m. Pre-calculation indicated that the resistance force on the blocking block was about 150 N, originating from the spring force. An external load opposing the motion direction was applied to the blocking block.

The simulation observes variations in mechanism performance under different parameters by altering the values of design variables. By comparing the sensitivity of design variables, it identifies the primary variables influencing mechanism performance. The design variables are listed in Table 2. In ADAMS, the measurement variable is set as MOTION_1_MEN_1.

With the simulation step size set to Steps=200, establish the measured torque value *T* as the optimization objective in the "Simulation/Design Evaluation" command to optimize the lengths of *a, b*, and *e*. During simulation, variables were changed individually to study the variation of driving torque *T* with the lengths of *a, b*, and *e*. Fifty sets of experiments were conducted within the variable ranges. Nine representative sets showing the change of driving torque *T* with variable a were selected, as shown in Table 3. The average sensitivity of driving torque *T* to the three variables is shown in Table 4.

Table 3

Change of the value of driving force distance *T* with *a*

Test No.	*T* (N·m)	*a* (mm)	Sensitivity
1	16.152	80	-21107
2	15.702	85	-2.1511
3	15.453	90	-2.2278
4	14.996	95	-2.2974
5	14.610	100	-2.3623
6	14.122	105	-2.4328
7	13.548	110	-2.4538
8	13.014	115	-2.4576
9	12.675	120	-2.4593

Table 4

Sensitivity of design variables

Design Variable	Sensitivity to Driving Torque
a	-2.28956
b	120.532
e	-104.77

Based on the data from Tables 3 and 4, among the three design variables, *a* has the lowest sensitivity to driving torque *T*, indicating it has a smaller influence on the driving torque. Variables *b* and *e* have a significant influence, making them the main factors affecting the change in driving torque.

Through ADAMS simulation analysis, with the torque on the trigger crank being 14.6 N·m, simulation of the trigger mechanism showed that when *a* = 100 mm, *b* = 30 mm, and *e* = 90 mm (integer values), and the force on the slider is 150 N, the output torque on the driving rocker is closest to 14.6 N·m. The design of the rotating crank connected to the shaft needs to be reasonable; it can be connected to the blocking rod via a connecting plate. Through design calculations and motion analysis, the rocker length was set to 100 mm. To prevent interference with the rocker of the rope-feeding mechanism, the rotating crank was approximated as a semicircle with a diameter of 100 mm.

Spring Dynamic Analysis and Selection

Calculated based on the minimum torque of the tines, the force the trigger mechanism can withstand at this moment reaches its maximum. The friction coefficient μ for straw-like materials is 0.4–0.47 *(Wang et al., 2017)*. According to the friction formula $F_f = \mu N$, where *N* is the weight of the reeds, the friction force $F_f = 15N$ generated by a full bin of reeds, which is small and negligible. The minimum force exerted by the tine on the reeds is *F*=915 N. The trigger crank is 8 cm above the base plate, so the force exerted by the tine on the reeds acting on the trigger crank is F_3=2*F*/5=366 N. Assuming uniform force distribution on the trigger crank, the force from the reeds acts at the centroid of the crank. The torque at this point, calculated using the torque formula, is M_3=14.64 N·m. Since the simplified crank 3 rotates simultaneously with the trigger crank, the torque magnitude is the same. The trigger crank is connected to the trigger mechanism via a shaft. The simplified force model of the trigger mechanism is shown in Fig. 6. With the rocker length *L* = 100 mm, *F* = 146.4 N is obtained. Therefore, calculated based on minimizing reed damage, the maximum force *F* required to pull the spring to the trigger position is 146.4 N.

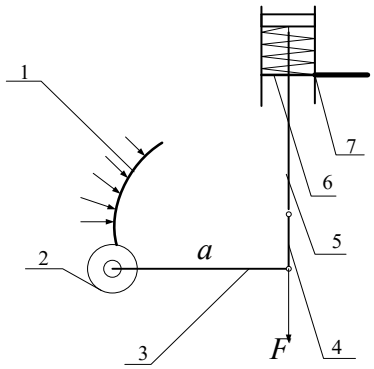

Fig. 6 – Trigger simplified model

1. Trigger crank 2. Shaft connection 3. Simplified crank 4. Connecting block 5. Blocking rod 6. Spring 7. Stop block bracket

The triggering mechanism requires a matching compression spring. The spring is crucial for determining whether triggering occurs. A spring with too low stiffness may cause premature triggering, reducing bale density, while excessive stiffness may lead to reed accumulation in the bin, potentially causing reed damage or failure to trigger. Therefore, spring selection must meet the following requirements: the distance between the blocking bracket and spring stop block is 100 mm, requiring a spring compression stroke $h > 15$ mm. To ensure that the spring meets operational and installation requirements, its free length H_0 should be $100 \leq H_0 \leq 140$ mm. The blocking rod diameter is 15 mm, requiring the spring inner diameter $D\text{-}d > 15$ mm. The spring stop block size is 50 mm × 50 mm, requiring the spring outer diameter $D+d < 50$ mm. The force $F = 146.4$ N. To minimize reed damage, the spring's maximum working load should be $110 \text{ N} \leq F \leq 146.4$ N. For comparative tests, a maximum working load $F < 170$ N was selected, i.e., the spring working load range is $110 \text{ N} \leq F \leq 170$ N. At this point, the spring compression equals the initial length H of 85 mm.

The spring's working load is the tension it experiences when pulled down to the trigger position. Different spring working loads result in different bale densities, affecting the net hourly productivity of the entire device. Subsequent experiments used different pre-tightening forces caused by the spring as a factor to verify the bale forming rate, bale density, and net hourly productivity of the baling device.

Single-Factor Experiment and Analysis of Pre-tightening Force

Reeds collected in November from the Zhuo River in Weifang City were used for this experiment. Collected reeds were trimmed according to the feeding port size of the test device, retaining the middle section of the reed stalks (1.2 m–2.6 m). The measured average moisture content was 20.7%, consistent with material test results. After multiple measurements using an electronic scale, the average weight of a single trimmed reed was approximately 13 g. Fig. 7 shows the prepared test materials.

Fig. 7 – Experimental materials

Fig. 8 – Binder test stand

The pre-tightening force is controlled by the spring in the triggering mechanism. The spring is the key component determining when baling is triggered. A higher spring stiffness (greater force) makes triggering harder, resulting in a higher weight per bale. Five springs with relatively evenly spaced maximum working loads were selected for the single-factor experiment. The experiment fixed the operating speed at 90 r/min and used nylon rope. Damage rate, bale forming rate, and single bale weight were evaluation indicators. Reeds were fed manually and uniformly during the test. The experiment was conducted synchronously with the single-factor speed test. After testing each spring, it was replaced before proceeding. The results for damage rate, bale forming rate, and single bale weight are shown in Table 5.

Table 5

Pre-tightening test results

Pre-tightening Force (N)	123	136.5	145.5	156	165
Damage Rate (%)	3.29	3.59	3.88	4.98	5.22
Single Bale Weight (kg)	4.14	4.31	4.44	4.51	4.55
Bale Forming Rate (%)	100	98	96	92	90

The test data shows that, under different spring conditions, a higher pre-tightening force results in higher bale density. This is because the reeds are compressed during baling and expand due to stress relaxation afterward. A higher pre-tightening force delays triggering, allowing more reeds to accumulate in the bin. Since the volume of the formed bale is similar, reeds expand more after baling with higher pre-tightening forces, leading to higher density. Net hourly productivity also increases with higher pre-tightening force. The pre-tightening force has a limited effect on bale density and forming rate. However, experiments showed that increased pre-tightening force caused more reed damage, with a higher number of surface creases in the formed bales compared to lower pre-tightening forces. Therefore, to ensure reed quality while meeting net hourly productivity and bale density requirements, springs resulting in higher productivity and density were selected. However, when the pre-tightening force increased from 145.5 N to 156 N, the damage rate increased sharply. Considering factors like damage rate, the pre-tightening force range was set at 123 N, 136.5 N, and 145.5 N.

Orthogonal Experiment for Reed Baling

Preliminary experiments indicated that the bale forming rate, bale density, damage rate, and other test results are related to rope type, motor operating speed, and spring pre-tightening force. Therefore, these three factors were used to establish an orthogonal experiment factor-level table, detailed in Table 6.

Table 6

Test factors and levels

Factor		Level		
		1	2	3
A	Rope Type (Diameter 1.5mm)	Hemp rope	Nylon rope	Cotton rope
B	Operating Speed (r/min)	80	90	100
C	Pre-tightening Force (N)	123	136.5	145.5

RESULTS

The results of the orthogonal experiment are shown in Table 7.

Table 7

Testing results and analysis

No.	Factor Level			Indicator Values		
	Rope Type A	Operating Speed B	Pre-tightening Force C	Net Hourly Productivity (t/h)	Damage Rate (%)	Bale Forming Rate (%)
1	1	1	1	0.548	3.38	99
2	1	2	2	0.561	3.68	96
3	1	3	3	0.573	3.97	93
4	2	1	1	0.547	3.28	100
5	2	2	2	0.56	3.59	98
6	2	3	3	0.574	3.86	96
7	3	1	2	0.55	3.62	97
8	3	2	3	0.563	3.9	95
9	3	3	1	0.571	3.34	100
10	1	1	3	0.549	3.98	93
11	1	2	1	0.559	3.39	100

No.	Factor Level			Indicator Values		
	Rope Type A	Operating Speed B	Pre-tightening Force C	Net Hourly Productivity (t/h)	Damage Rate (%)	Bale Forming Rate (%)
12	1	3	2	0.574	3.66	97
13	2	1	2	0.549	3.55	98
14	2	2	3	0.564	3.88	96
15	2	3	1	0.573	3.29	100
16	3	1	3	0.548	3.92	95
17	3	2	1	0.562	3.36	100
18	3	3	2	0.575	3.63	98

Variance analysis was performed on the experimental data, and the results are presented in Table 8. Analysis of Table 8 reveals that since the P-values for rope type, operating speed, and pre-tightening force are all less than 0.05, these factors exhibit statistically significant effects on the target metrics. Further comparison of the F-values in the ANOVA indicates the following primary-secondary order of influencing factors: For net hourly productivity: B (Operating Speed) > C (Pre-tightening Force) > A (Rope Type). For damage rate: C (Pre-tightening Force) > A (Rope Type) > B (Operating Speed). For bale forming rate: A (Rope Type) > C (Pre-tightening Force) > B (Operating Speed).

Table 8

ANOVA Results

Source	Dependent Variable	Type III Sum of Squares	df	Mean Square	F	Sig.
Intercept	productivity	5.667	1	5.667	3319852.071	0.000
	Damage rate	236.749	1	236.749	1370650.947	0.000
	Bundling rate	170333.389	1	170333.389	475014.239	0.000
A	productivity	2.111×10^{-6}	2	1.056×10^{-6}	.618	0.047
	Damage rate	0.031	2	0.016	89.833	0.000
		8.778	2	4.389	12.239	0.002
B	productivity	0.002	2	0.001	542.287	0.000
	Damage rate	0.000	2	0.000	1.254	0.033
	Bundling rate	0.778	2	0.389	1.085	0.032
C	productivity	1.144×10^{-5}	2	5.722×10^{-6}	3.352	0.043
	Damage rate	1.004	2	0.502	2905.254	0.000
	Bundling rate	80.111	2	40.056	11.704	0.000
Error	productivity	1.878×10^{-5}	11	1.707×10^{-6}		
	Damage rate	0.002	11	0.000		
	Bundling rate	3.944	11	0.359		
Total	productivity	5.669	18			
	Damage rate	237.786	18			
	Bundling rate	170427.000	18			
Corrected Total	productivity	0.002	17			
	Damage rate	1.037	17			
	Bundling rate	93.611	17			

For Rope Type (A), level 2 (Nylon rope) yields the lowest damage rate (3.575%) and highest bale forming rate (98.0%). Thus the Nylon rope is optimal. For Operating Speed (B), damage rate (3.622–3.633%) and bale forming rate (97.0–97.5%) show minimal variation across levels. Level 3 (100 r/min) achieves the highest net hourly productivity (0.573 t/h). Thus 100 r/min is optimal. For Pre-tightening Force (C), level 1 (123 N) delivers the lowest damage rate (3.340%) and highest bale forming rate (99.833%). Thus 123 N is optimal. The optimal parameter combination is Nylon rope, 100 r/min operating speed, and 123 N pre-tightening force.

CONCLUSIONS

(1) This study developed a triggering rope-feeding mechanism for a reed bundling device. Its core innovation lies in employing a rocker-slider mechanism combined with springs to achieve automatic triggering, while utilizing a crank-rocker mechanism to drive the hollow rope-feeding needle. The mechanism initiates the bundling process by sensing accumulated reed weight. During operation, the rope-feeding needle simultaneously performs three critical functions: routing the rope into the knotter, compressing reeds to enhance bundle tightness, and blocking subsequent reed retraction. This provides a foundational mechanical solution for efficient and low-damage whole-stalk reed bundling.

(2) Based on ADAMS, parameterized simulation optimization of the triggering mechanism is carried out, and the key influencing factors of the rod length parameters *b* and *e* are determined through sensitivity analysis of the driving torque to obtain the optimal rod length combination. Based on the analysis of spring dynamics, the critical value of spring working load of 146.4 N and selection parameters were established, providing a design basis for reducing the driving torque of the mechanism and mitigating reed damage.

(3) The influence of rope type, working speed, and pre tension on bundling performance was verified through orthogonal experiments: working speed has the most significant impact on pure working hour productivity, pre tension dominates damage rate, and rope type determines bundling rate. The optimal combination is nylon rope, working speed of 100 r/min, and pre tension force of 123 N, achieving low damage and efficient bundling of reed whole poles.

REFERENCES

[1] Cen Haitang, Song Yu, Wei Ruitao, Li Ling, Qin Jianbin (2020). Reliability Design of Knotter Cam Gear for D-type Knotter. *IOP Conference Series: Materials Science and Engineering*, Vol. 784 no.1, pp. 012020, doi:10.1088/1757-899X/784/1/012020;

[2] Chen Kesheng (2020). *Design and Research of Reed Compression Characteristics and Compression Packing Device (芦苇压缩特性及其压缩打包装置设计与研究).* Master's Thesis, Shihezi University, doi:10.27332/d.cnki.gshzu.2020.000290;

[3] Chen Longjian, Li Cheng, Zhang Anqi, Li Haitao, Zhang Shaoying (2015). Load Test Analysis of Knotter Jaw During Straw Baling Process (秸秆捆扎过程中打结钳嘴载荷试验分析). *Transactions of the Chinese Society for Agricultural Machinery*, Vol. 46 no.9, pp. 128-134, doi: 10.6041/j.issn.1000-1298.2015.09.019;

[4] Zhong Chengyi, Yin Wenqing, Liu Dejiang, Yao Keheng, Chen Wei, Xing Zitao, Jin Fan (2023). Design and experiment of self-propelled highland barley harvesting and baling machine. *INMATEH-Agricultural Engineering,* Vol. 70 no.2, pp. 423-430, doi: https://doi.org/10.35633/inmateh-70-41;

[5] Du Tuo, Li Yaoming, Yin Qiang, Ji Binbin (2024). Static and Modal Analysis of Reed Clamping Conveying Device Frame (芦苇夹持输送装置台架的静力学及模态分析). *Journal of Agricultural Mechanization Research*, Vol. 46 no.8, pp. 70-74, doi: 10.13427/j.cnki.njyi.2024.08.023;

[6] Flick D., Nigon M. C., Shinners K.J. Friede J. C. (2019). Control system for a continuous compaction large square baler. *Computers and Electronics in Agriculture,* Vol. 2 no.7, pp.519-528, doi: https:// 10.1016/j.compag.2019.104969;

[7] He Ming (2017). *Design Research of Baling Device for Rapeseed Binding Harvester (油菜割捆机打捆装置的设计研究).* Master's Thesis, Hunan Agricultural University*;*

[8] Li Yancong, Wang Yonghong, Guo Junwang, Li Shuhuan, Wei Yong (2021). Simulation Design of Ree d Harvester Rake Mechanism (芦苇收割机拨齿机构仿真设计). *Journal of Agricultural Engineering*, Vol.11 no.6, pp. 94-98, doi: 10.3969/j.issn.2095-1795.2021.06.021;

[9] Li Yancong, Wei Yong, Zhang Hao, Song Xin, Liu Yule (2020). Design and Kinematic Analysis of Key Components for Reed Harvester (芦苇收割机关键部件设计及运动分析). *Journal of Chinese Agricultural Mechanization*, Vol. 41 no.12, pp. 20-23, doi:10.13733/j.jcam.issn.2095-5553.2020.12.005;

[10] Nalobina O., Holotiuk M., Bundza O., Shymko A., Puts V., Martyniuk V. (2024). Machine for technological spring harvesting of technical hemp, *INMATEH-Agricultural Engineering,* Vol. 74 no.3, pp. 25-32, doi: https://doi.org/10.35633/inmateh-74-02;

[11] Wang Defu, Jiang Zhiguo, Li Baiqiu, Wang Guofu, Jiang Yiyuan (2017). Experiment on Sliding Friction Characteristics Between Rice Straw and Baler Steel-Roll (稻秆与圆捆机钢辊间滑动摩擦特性试验). *Transactions of the Chinese Society of Agricultural Engineering (Transactions of the CSAE)*, Vol. 33 no.21, pp. 44-51, doi: 10.11975/j.issn.1002-6819.2017.21.005;

[12] Wang Haichao, Sun Xiaotian, Liu Yu, Pei Zhiyong, Guo Gensheng (2021). Motion Simulation Analysis and Optimization of Feeding Mechanism for 4YF-1300 Large Square Baler Based on MATLAB (基于 MATLAB 的 4YF-1300 型大方捆打捆机喂入机构运动仿真分析与优化). *Journal of Chinese Agricultural Mechanization*, Vol. 42 no.2, pp. 31-36, doi:10.13733/j.jcam.issn.2095-5553.2021.02.005;

[13] Wang Qi, Li Chenqi, Zhang Xuesong, Wang Chunming, Pan Yufeng (2023). Application and Development Trend of Reed Fiber Materials (芦苇纤维材料的应用及发展趋势). *Forestry Science and Technology*, Vol. 48 no.5, pp. 60-62, doi: 10.19750/j.cnki.1001-9499.2023.05.014;

[14] Wang Xiang, Gao Lei, Bao Zhiliang, Guo Xiyan, Meng Yu (2025). Design and Experiment of Feeding Mechanism for Square Baler Based on SolidWorks (基于 SolidWorks 的方捆机喂入机构设计与试验). *Journal of Chinese Agricultural Mechanization*, Vol.46 no.2, pp.35-40+47, doi: 10.13733/j.jcam.issn.2095-5553.2025.02.006;

[15] Yin Qiang, Li Yaoming, Ji Binbin, Chen Lipeng (2023). Design and Experiment of Clamping Conveying Device for Self-Propelled Reed Harvester (自走式芦苇收获机夹持输送装置的设计与试验). *Journal of Agricultural Mechanization Research*, Vol. 45 no.4, pp. 113-118, doi:10.13427/j.cnki.njyi.2023.04.046;

[16] Zhang Fu, Lou Limin, Qian Dan, Wang Shiqiang, Feng Chunling, Zhao Yirong (2024). Optimum design and test of compression mechanism of big square baler (大方捆打捆机压缩机构优化设计及试验). *Journal of Jilin University (Engineering and Technology Edition)*, Vol. 54 no.4, pp. 1166-1174, doi: 10.13229/j.cnki.jdxbgxb.20221139;

[17] Zhang Xiaojun (2024). Motion Simulation and Experiment of Compression Mechanism for Six-Twine Large Square Baler (六道捆绳大方捆打捆机压缩机构运动仿真与试验). *Journal of Agricultural Equipment and Vehicle Engineering*, Vol. 62 no.12, pp. 29-32;

[18] Zhao Xue (2021). *Modification of reed and its design application in furniture decoration (芦苇茎秆改性及其在家具装饰设计中的应用研究).* Doctoral Dissertation, Beijing Forestry University, doi: 10.26949/d.cnki.gblyu.2021.000990.